metals

MDPI

Article

Low Cycle Fatigue Behaviors of Alloy 617 (INCONEL 617) Weldments for High Temperature Applications

Rando Tungga Dewa [1], Seon Jin Kim [1,*], Woo Gon Kim [2] and Eung Seon Kim [2]

[1] Department of Mechanical Design Engineering, Pukyong National University, Busan 608-739, Korea; rando.td@gmail.com

[2] Korea Atomic Energy Research Institute (KAERI), Daejeon 305-353, Korea; wgkim@kaeri.re.kr (W.G.K.); kimes@kaeri.re.kr (E.S.K.)

* Correspondence: sjkim@pknu.ac.kr; Tel.: +82-51-629-6163; Fax: +82-51-629-6250

Academic Editor: Giuseppe Casalino

Received: 15 March 2016; Accepted: 25 April 2016; Published: 28 April 2016

Abstract: In this study, we comparatively investigate the low cycle fatigue behavior of Alloy 617 (INCONEL 617) weldments by gas tungsten arc welding process at room temperature and 800 °C in the air to support the qualification in high temperature applications of the Next Generation-IV Nuclear Plant. Axial total-strain controlled tests have been performed with the magnitude of strain ranges with a constant strain ratio ($R_\varepsilon = -1$). The results of fatigue tests consistently show lower fatigue life with an increase in total strain range and temperature at all testing conditions. The reduction in fatigue life may result from the higher cyclic plastic strain accumulation and the material ductility at high temperature conditions. A constitutive behavior of high temperature by some cyclic hardening was observed. The occurrence of serrated yielding in the cyclic stress response was also observed, suggesting the influence of dynamic strain aging during high temperature. We evaluated a well-known life prediction model through the Coffin-Manson relationship. The results are well matched with the experimental data. In addition, low cycle fatigue cracking occurred in the weld metal region and initiated transgranularly at the free surface.

Keywords: alloy 617; low cycle fatigue (LCF); gas tungsten arc welding (GTAW); weldment; high temperature; dynamic strain aging (DSA); life prediction; fracture behavior

1. Introduction

The very high temperature reactor (VHTR) is one of the most promising nuclear systems among the Generation-IV reactors to economically produce electricity and hydrogen. The VHTR major components include the reactor internals, reactor pressure vessel, piping, hot gas ducts (HGD), and intermediate heat exchangers (IHX). These components are required to have good mechanical properties, creep-fatigue resistance, and phase stability at high temperatures. There have been no materials approved by ASME Section III Subsection NH which is a nuclear code for temperatures reaching 1000 °C. Currently, Alloy 617 is the leading candidate material to prolong the design life of IHX and HGD of helium-cooled VHTR systems due to its creep-fatigue resistance at high temperatures [1–3].

Nowadays, the Korea Atomic Energy Research Institute (KAERI) is developing a nuclear hydrogen development and demonstration plant with a capacity of 200 MW_{th} with thermal and core outlet temperature of 950 °C [1,2,4,5]. The components have a projected plant design service life of 40–60 years operation and 3–8 MPa in He impurities. The most important consideration is the creep-fatigue and fatigue behavior of the materials, especially in welded structure [3–5]. The Alloy 617 for the IHX and other components is expected to operate at room temperature, which is assumed as a start-up condition, and at temperatures between 800–950 °C.

Low cycle fatigue (LCF) loading is expected to be an important damage mode for the IHX as a result of operating conditions that generate power transients and a temperature-gradient induced from thermal strain during operation as well as startups, shutdown work and load fluctuating, each of which produces cyclic loading [3]. The consideration could be used to determine material resistance against the cyclic loading. For mechanical structures, welded components are necessary and some of the components are joined using various welding techniques. Therefore, weldments are unavoidable and may have several inherent defects. It is necessary to understand fatigue damage of weldments, because it is more brittle than base metal (BM), and it is micro-structurally and mechanically heterogeneous, which could form a source of fatigue failures [4–6].

Many attempts have been made in the past two decades to evaluate the LCF and/or creep-fatigue behavior in Alloy 617 BM and weldments at ambient and elevated temperatures [3,7–14]. Based on their results, it is very difficult to separate the effects of temperature, strain rate and environment as they have complex interrelationships. However, they did not investigate the LCF behavior of the weldments as a comparative study at room temperature and 800 °C thermal conditions over different total strain ranges as investigated in this study, and also at a specific rate of change in strain deformation. It is important to provide a baseline data of the LCF properties of weldments to ensure the reliability of welded structures.

To support the modeling and understanding of the LCF behavior of Alloy 617, weldments was made from gas tungsten arc welding (GTAW) butt-welded plates. In this paper, KAERI and Pukyong National University (PKNU) investigate the LCF behavior for Alloy 617 weldments, in order to provide the commencement of high temperature LCF behavior. We performed an initial strain-controlled LCF test in air at room temperature and 800 °C under different total strain ranges of 0.6, 0.9%, 1.2% and 1.5%, and with a constant strain ratio ($R_\varepsilon = -1$), and the results were consistent with those listed from ASTM Standard E606 [15]. The tensile test measurements were first done as a reference data for Alloy 617 weldments for better understanding and explanation of fracture behavior [4]. The microscopic investigations were also examined with selected specimens to compare LCF fracture behavior of Alloy 617 weldment specimens.

2. Materials and Methods

2.1. As-Received Alloy 617 Weldments

Figure 1 shows the cross-view of etched Alloy 617 weldments microstructure. The microstructure consisted of BM with well-uniformed equiaxed grains, following the heat affected zone (HAZ) structure with a fusion line and coarser grain boundaries. Lastly, the dendritic structure was formed in the weld metal (WM) region because of the solidification during the welding process. The chemical composition of the as-received Alloy 617 used in the present study is shown in Table 1. The shape of the weldments has a single V-groove with an angle of 80° and 10 mm root gap from a 25 mm thick rolled plate. A filler metal was used for KW-T617. It was prepared according to AWS specifications, AWS A 5.14-05 ERNiCrMo-1 (UNS N06617), and the diameter was 2.4 mm. In order to prevent a bending deformation of the weldments, some passes to the back side were added for each specimen. A post heat treatment was not conducted because a Ni-based superalloy is not normally applied. After the welding process, the soundness of the weldments was qualified through an ultrasonic test (UT), a tensile test, and a bending test. The bending testing results coincide well with ASME specifications, which means the micro-crack is within 3.2 mm. It was also observed that the weldments exhibited acceptable ductility. Nevertheless, the soundness of the weldments has no problems.

LCF and tensile weldment specimens were machined from a weld pad in the transverse direction against the welding direction as shown in Figure 2a. The cross section of the weld specimen involves a gage length, consisting of WM and HAZ materials only: the WM is in the center of the section and two HAZs are next to it. For further details, Figure 2b shows the shape and dimension of the LCF specimen with 6.0 mm diameter in the reduced section with a parallel length of 18 mm and a gauge length of

12.5 mm. However, the flat tensile test specimens were machined into a rectangular cross section with a gage length of 28.5 mm, width of 6.25 mm, and thickness of 1.5 mm.

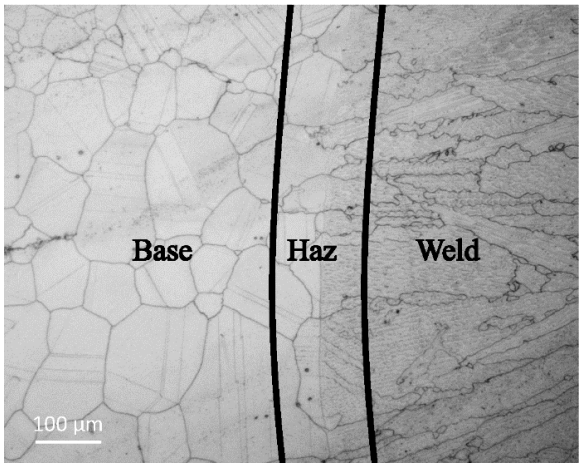

Figure 1. Microstructure of the cross-view for Alloy 617 weldments.

Table 1. The chemical composition of Alloy 617 plate (wt. %).

		C	Ni	Fe	Si	Mn	Co	Cr	Ti	P	S	Mo	Al	B	Cu
ASTM Spec	Min	0.05	Bal.	-	-	-	10	20	-	-	-	8	0.8	-	-
	Max	0.15	Bal.	3.0	1.0	1.0	15	24	0.6	0.015	0.015	10	1.5	0.006	0.5
Alloy 617	-	0.08	53.11	0.95	0.08	0.03	12.3	22	0.41	0.003	<0.002	9.5	1.06	<0.002	0.027

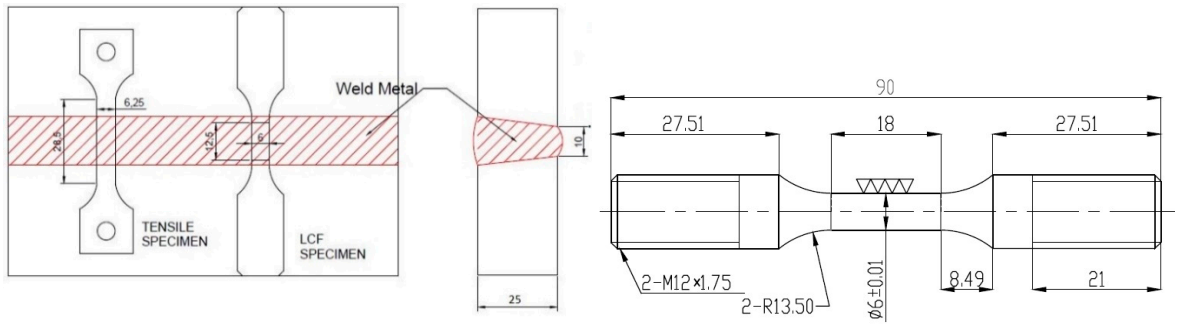

(**a**) (**b**)

Figure 2. (**a**) The weld pad configuration of weldment specimens; (**b**) The cylindrical low cycle fatigue (LCF) specimen's shape and geometry.

2.2. Experimental Methods

We conducted fully reversed ($R_\varepsilon = -1$) total axial strain-controlled LCF tests of Alloy 617 weldments in air environment by using a servo hydraulic machine (Instron 8516 capacity 100 kN, Instron Korea, Seoul, Korea) under 0.25 Hz constant frequency regarding four total strain ranges of 0.6%, 0.9%, 1.2%, and 1.5% at room temperature and 800 °C. The strain rate was varied from 3×10^{-3} s^{-1} to 7.5×10^{-3} s^{-1} depending on total strain range. We use a closed loop servo hydraulic system equipped with a tube furnace and three temperature controllers on the top, center, and bottom region. Therefore, the temperature was remained within 800 °C ± 2 °C of the nominal temperature throughout the test. The specimen was held at a target temperature with zero load for about 30 min to allow temperatures to stabilize before the commencement of the test. We applied triangular waveforms with equal push-pull mode to specimens. As in the literature review [3,9,10,15], we also defined the

failure criteria as the number of cycles, which means a 20% level drop off from the initial level of the peak tensile stress. We used a personal computer through a high precision extensometer with 12.5 mm gage length that was attached to the gauge section of the specimen. The gauge section mainly covers the weld and HAZ materials only, to produce a strain/time records as well as load/time records and load/strain loops of each test condition.

In order to examine the LCF fracture morphologies, we investigated the post fracture analysis of the selected specimens which interrupted into two pieces in preliminary observation by using high magnification scanning electron microscopy (SEM Hitach JEOL JSM 5610, JEOL Korea Ltd., Seoul, Korea) and optical microscopy (OM Olympus GX-51, Olympus Korea Co. Ltd., Seoul, Korea). We prepared the specimens for OM observations by cutting them into two parts. The cutting surfaces were polished after mounting and they were sequentially etched in solutions of hydrochloric acid, ethanol, and copper II chloride. The tensile tests have been first done as a reference data for better understanding and explanation of fracture behavior, with a strain rate of 5.85×10^{-4} s^{-1}. Table 2 shows the results of the tensile tests for Alloy 617 weldments. However, it is notable that the increase in temperature resulted in a lower yield stress (YS) and the ultimate tensile strength (UTS) values, although the tensile elongation (or material ductility) slightly increases with increasing temperature.

Table 2. The results of tensile tests on Alloy 617 weldments.

Temperature (°C)	YS (MPa)	UTS (MPa)	EL (%)
Room temperature	462	764.9	24.6
800 °C	314	382.7	27.3

3. Results and Discussion

3.1. Low Cycle Fatigue Behaviors of Alloy 617 Weldments

The fatigue resistance can be considered as: the microstructural or material property, the fatigue rate, and the temperature influence. We listed a summary of the results in Table 3. Most of the test results show that the increasing of strain range and temperature condition resulted in a reduction of fatigue life. At room temperature condition shows a comparatively higher cyclic stress response with increasing strain ranges compared to the 800 °C testing conditions, although the plastic strain accumulation of the 800 °C testing conditions is comparatively higher. From the results, we can deduce that the higher plastic strain deformation and the material ductility of the 800 °C testing conditions to have a major role in the shorter fatigue life.

Table 3. Summary of LCF tests results of Alloy 617 weldments.

Specimen Reference		Cycles to Failure	Elastic Strain Amp (mm/mm)	Plastic Strain Amp (mm/mm)	Stress Amp (MPa)
Temperature	Total Strain Amp (mm/mm)				
Room temperature	0.0075	416	0.0037	0.0038	665.9
	0.0060	1485	0.0033	0.0027	656.2
	0.0045	2924	0.0029	0.0016	621.1
	0.0030	28422	0.0027	0.0003	545.6
800 °C	0.0075	230	0.0034	0.0041	566.3
	0.0060	334	0.0034	0.0026	565.3
	0.0045	655	0.0029	0.0016	523.9
	0.0030	3282	0.0026	0.0004	417.2

In engineering, materials usually exhibit cyclic hardening or softening to some level in the cyclic plastic deformation process. Figure 3 shows the cyclic stress response curves with respect to the number of cycles regarding four total strain ranges under continuous cyclic loading. The cyclic stress

response at room temperature conditions showed a cyclic softening region for the major portion of the life after a short period of initial hardening. The short period of cyclic initial hardening was observed for about 2–200 cycles, and remained during the softening phase until failure. At the lowest strain range (0.6%), the saturation region was also observed. Dissimilar cyclic stress response behavior was found in both temperature conditions. However, the results at 800 °C distinctly showed a cyclic hardening for the major portion of the fatigue life. At the end of the test, the cyclic stress response decreased rapidly, which indicates the initiation of a macro-crack.

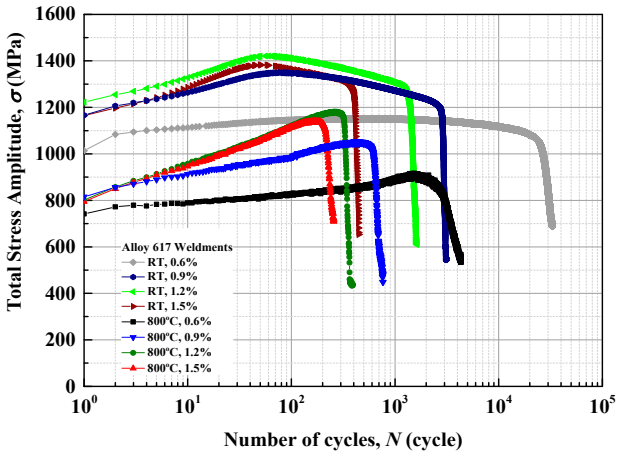

Figure 3. The cyclic stress response curves regarding to four total strain ranges under continuous cyclic loading for Alloy 617 weldments.

In order to clearly understand the relationship between cyclic stress response and crack behavior, Figure 4 shows the normalized stress amplitude on the fraction of fatigue life, which was used to deduce the number of cycles regarding macro-crack initiation, N_i. The fraction of fatigue life is the ratio between the number of cycles and the total cycles to failure. We defined the crack initiation as the point at which the stress amplitude rapidly decreased from an initial trend. From the figure, the profile significantly shows that the crack initiation occurs earlier at approximately 90% of the total cycles to failure. Meanwhile, at 0.6% total strain range, it was occurred in approximately 60% of the total cycles to failure, and remained during propagation life. It is noted that, under low total strain range, the fatigue crack propagation occurred earlier and it is particularly important to overall fatigue life when it is utilized in the high temperature condition.

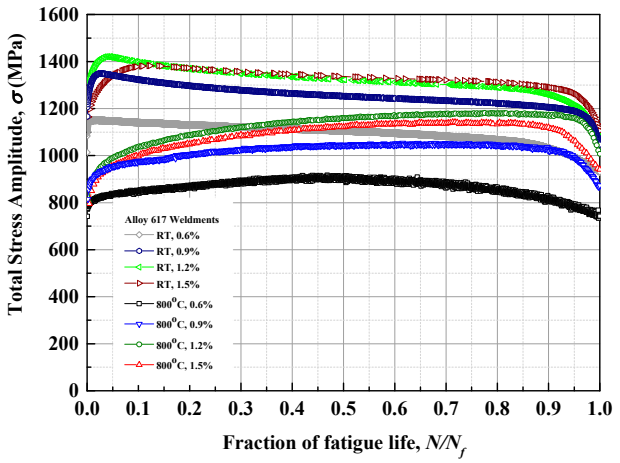

Figure 4. The normalizing fatigue life on cyclic stress response regarding to four total strain ranges of Alloy 617 weldments at room temperature and 800 °C.

In this study, we found that the work hardening behavior is an effect of initial cyclic hardening. Figure 5 shows the summary of cyclic stress-plastic strain curves of Alloy 617 weldments. From this graph, we can find that the stress increases with increasing plastic strain. In order to quantitatively determine the work hardening behavior, the Ramberg-Osgood equation is adopted:

$$\frac{\Delta\epsilon_T}{2} = \frac{\Delta\epsilon_P}{2} + \frac{\Delta\epsilon_e}{2} = \frac{\Delta\sigma}{E} + \left(\frac{\Delta\varepsilon_p}{2K'}\right)^{n'} \quad (1)$$

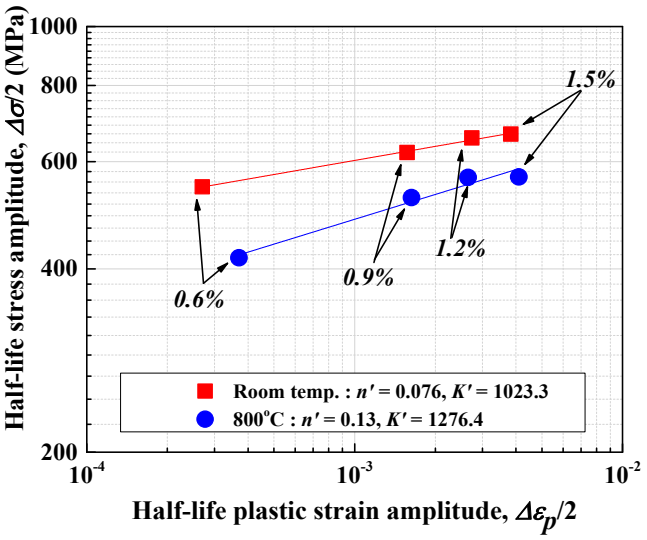

Figure 5. The cyclic stress-plastic strain curves of Alloy 617 weldments at room temperature and 800 °C.

The results are also given in Figure 5, where, K' and n' are cyclic strength coefficient and cyclic strain hardening exponent, respectively. From this figure, K' and n' were determined from the log-log relationships between half-life value (stable condition) of stress amplitude and plastic strain amplitude. The work hardening tendency of the weldments linearly increased through the whole total strain range conditions. However, the degree of work hardening of Alloy 617 weldments depends on the stress amplitude and the plastic strain value.

In this manifestation, we recognized the occurrence of dynamic strain aging (DSA) at 800 °C regarding four total strain ranges under continuous cyclic loading. The results showed a transformation of work hardening at 800 °C. DSA (sometimes termed as Portevin Le-Chatelier effect) is the hardening mechanism, which manifests itself by fluctuating or serration plastic flow. In the manifestation of DSA, we synchronously noticed the serrated flows on the tension-compression stresses at all testing conditions. Figure 6 shows the tensile peak stresses tested at 800 °C that exhibit serrations as a result of the locking-unlocking interactions of moving atoms. Meanwhile, J.-D. Hong *et al.* [16] revealed that the cyclic hardening might be increased with the occurrence of the DSA, and the ratio of the cyclic hardening could be used to evaluate the degree of DSA. Therefore, Figure 7 shows the ratio of cyclic hardening measured by the ratio of the maximum stress amplitude (σ_{peak}) to the stress amplitude of the first cycle ($\sigma_{initial}$). From the figure, it is obvious that the ratio of cyclic hardening increases along with the transformation of LCF test environment from previous work [4,5] at room temperature to the present investigation at 800 °C. As in the literature survey [11], they also acknowledged that the DSA occurs in the temperature range of about 650–900 °C for this Alloy 617.

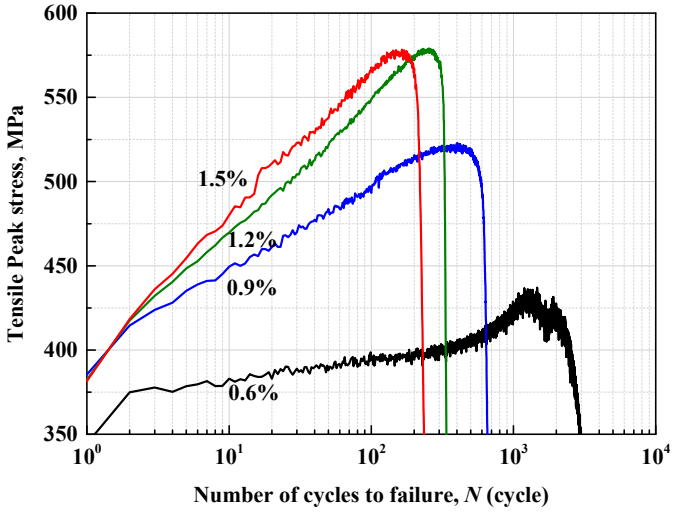

Figure 6. The serrated flows in the tensile peak stress curves of Alloy 617 weldments at 800 °C.

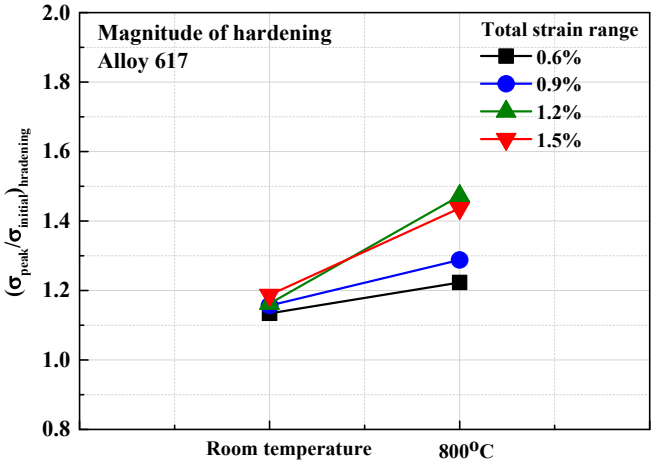

Figure 7. The comparison of ratio of cyclic stress amplitude as a magnitude of hardening of Alloy 617 weldments at room temperature and 800 °C.

3.2. Low Cycle Fatigue Life Prediction

Many scientists have made an enormous effort in order to predict the lifetime of metallic materials at elevated temperatures. The state of the art suggests that an issue has been addressed mainly in terms of strain. Plastic deformation is expected to play a major role in this process. Several researchers, e.g., Lazzarin, *et al.* and Susmel, *et al.* [17,18], have primarily considered a very high-temperature fatigue problem with the high cycle fatigue regime. This was initiated from the pioneering Coffin-Manson relationship as a definition of strain elements at LCF regime. In this issue, an appropriate life assessment using a conventional Coffin-Manson relationship is proposed for designing against the LCF of Alloy 617 weldments. The combining Coffin-Manson equation, better known as the strain-life relationship, is a function of the total strain range, $\Delta\varepsilon_T$, and the number of cycles to failure, N_f, by a similar power law function. The total strain as a dependence parameter can be separated into the plastic and elastic strain ranges and expressed by:

$$\frac{\Delta\epsilon_T}{2} = \frac{\Delta\epsilon_P}{2} + \frac{\Delta\epsilon_e}{2} = \frac{\sigma'_f}{E}\left(2N_f\right)^b + \varepsilon'_f\left(2N_f\right)^c \quad (2)$$

where, $\Delta\varepsilon_T/2$ is the total strain amplitude, $\Delta\varepsilon_e/2$ is the elastic strain amplitude, $\Delta\varepsilon_p/2$ is the plastic strain amplitude, $2N_f$ is the number of reversals to failure. σ_f' is the fatigue strength coefficient, b is the fatigue strength exponent, ε_f' is the fatigue ductility coefficient, c is the fatigue ductility exponent and E is the elastic modulus.

Figure 8a,b show the variety of LCF lives plotted with total strain ranges in the continuous cycling of the Alloy 617 weldment specimens at room temperature and 800 °C, respectively. These data were analyzed by means of the least squares fit method. In both logarithmic coordinates, the strain-life curves were simply fitted and they are related to Equation (2). The coefficients and exponents in the Coffin-Manson equation were determined, and are listed in Table 4. As previous works reported [3,15], when it was plotted on a log-log scale, the c slope typically may vary from −0.5~−1.0. The authors also reported the exponent c of −1.12 of Alloy 617 weldments at 800 °C, and it can be concluded that the value is comparable in the present study. From the figure, the transition of fatigue life in reversals ($2N_t$) represents the intersection of the elastic and plastic straight lines which means the stabilized hysteresis loop has equal plastic and elastic strain components. From this point to the left, where the fatigue life is lower than the transition, the fatigue life of the material is mainly dominated by ductility. Otherwise, where the fatigue life is higher than the transition, is controlled by the strength. Table 5 lists the transition of fatigue life at room temperature and 800 °C. From the results could be assumed that the strain amplitude at the transition life decreases with increasing temperature.

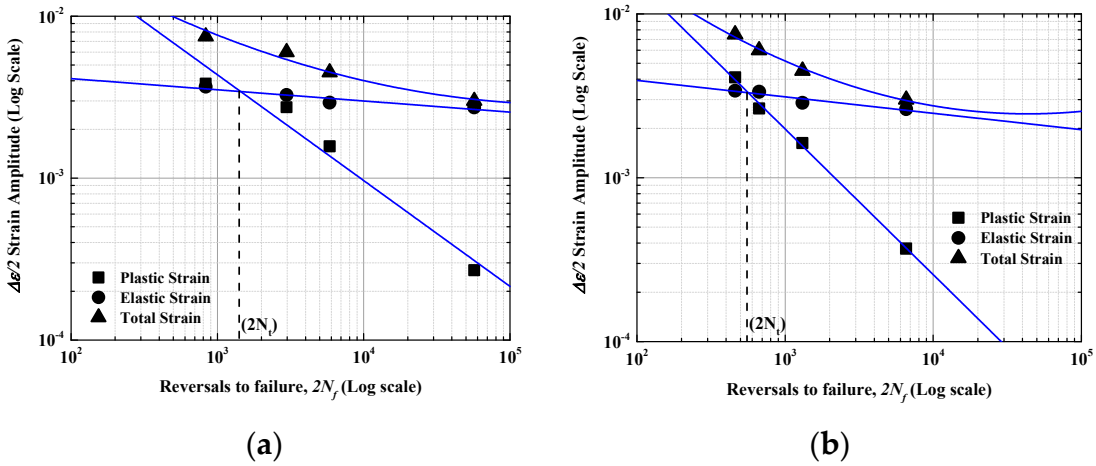

Figure 8. The Coffin-Manson curves of Alloy 617 weldments at (**a**) Room temperature; (**b**) 800 °C condition.

Table 4. Coefficients and exponents of Alloy 617 weldments in the Coffin-Manson equation.

Temperature	ε_f'	c	σ_f' (MPa)	b	E (GPa)	n'	K' (MPa)
Room temperature	0.398	−0.654	1213	−0.104	214.4	0.118	1086.43
800°C	0.924	−0.889	973	−0.100	155.9	0.14	1276.4

Table 5. The transition of fatigue life of Alloy 617 Weldments at room temperature and 800 °C.

Temperature	$2N_t$	$\Delta\varepsilon/2$
Room temperature	1410	0.0035
800°C	554	0.0033

In the process of the validation of the predicted life, Figure 9 shows the experimental data which are compared to the predicted lives by the Coffin-Manson relationship. Figure 9 shows a good correlation between the predicted and experimental fatigue lives. The validations are in good

agreement within a factor of 2.0. An excellent correlation can be observed for the Coffin-Manson relationship with 86.37% of accuracy.

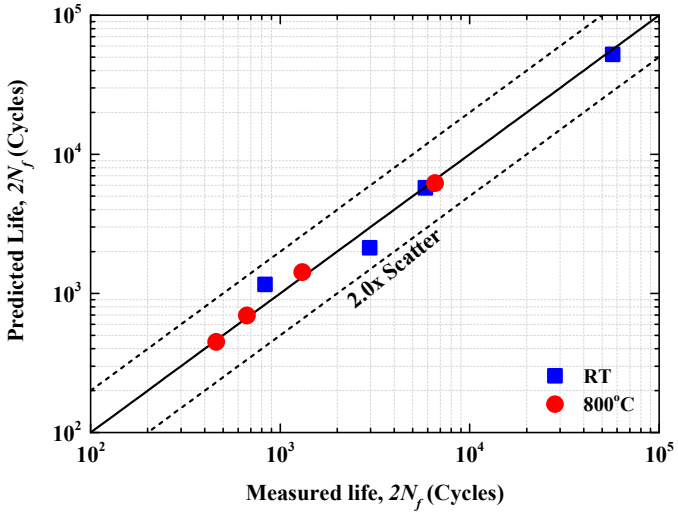

Figure 9. Validation of the predicted lives by Coffin-Manson relationship for Alloy 617 weldments.

3.3. Fracture Morphologies of Alloy 617 Weldments

Regardless of the effect of temperature, the fracture surface morphologies of the weldments at room temperature and 800 °C are very similar, as shown in Figure 10. From previous work [4], the weldments showed a relatively wedge-type crack with some deviations oriented at 45°to the loading direction. Figure 10 also shows the fractured specimens, which indicates the failure occurring inside of the gauge section in the WM region. Therefore, we denote that the possible weak spot is in the WM area of the weldments. However, the possible weakness of the WM as well as the presence of microstructural heterogeneity, and also the WM zone was comprised of large columnar grains with dendritic structure. A large plastic strain thereby accumulates, depending upon the material strength of individual microstructure, which could become a source of fatigue failures. In addition, the results of hardness measurement on the WM showed a lower value than that of the HAZ, but still higher than the BM.

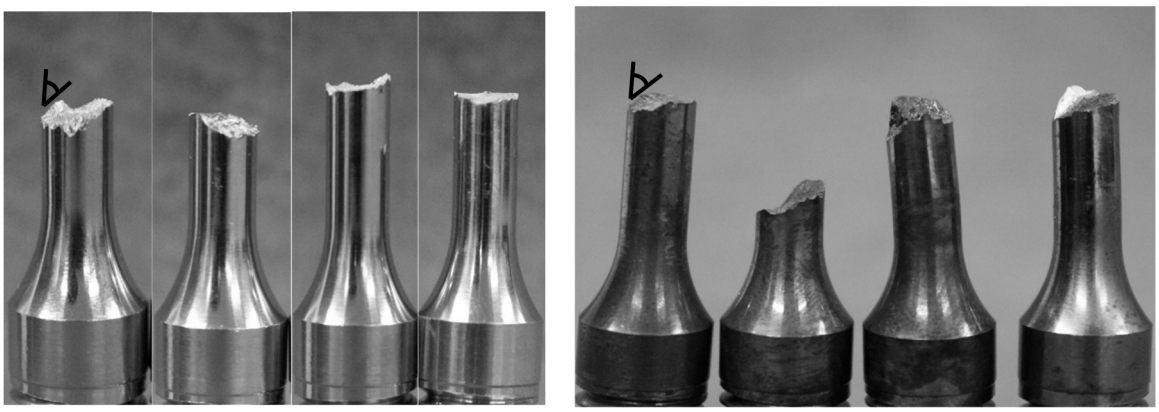

(**a**) (**b**)

Figure 10. Comparison of the fracture surface morphologies of Alloy 617 weldments at: (**a**) Room temperature; (**b**) 800 °C condition. From left to right *i.e.*, total strain range of 0.6%, 0.9%, 1.2%, 1.5%.

In nickel based Alloy 617 [6–12], a reduction of fatigue life was attributed to creep, oxidation, and DSA at elevated temperature. In this study, however, the difference in fatigue resistance cannot be fully interpreted by an effect of fracture morphology. In the regime of DSA, there were no evidences of creep and less effect of oxidation to account for the difference in the fatigue life with temperature in the present investigation. Figure 11a–d show a typical micrograph of the Alloy 617 weldment specimens at room temperature and 800 °C, respectively, which also show a transgranular crack initiation and propagation along with the interdendritic paths. Hong *et al.* [19] stated that the fatigue crack initiation is related to the plastic strain localization on the slip bands. The slip bands that contain extrusions, and intrusions, if connected to the surface, will lead to the production of crack initiation. Crack initiation occurred along slip planes, and this was evidenced by the cleavage facets in Figure 11c (stage I). This mechanism resulted in multiple points of the crack initiation site on their surfaces, and reduced the crack initiation life. This type continued through only a few grains, and transformed into stage II transgranular cracking. Figure 11d shows the fatigue striations that occurred on the fracture surface during crack propagation. Since DSA-induced work hardening process may cause the rapid crack propagation due to atoms interactions, the fatigue life also will decrease in the regime of DSA.

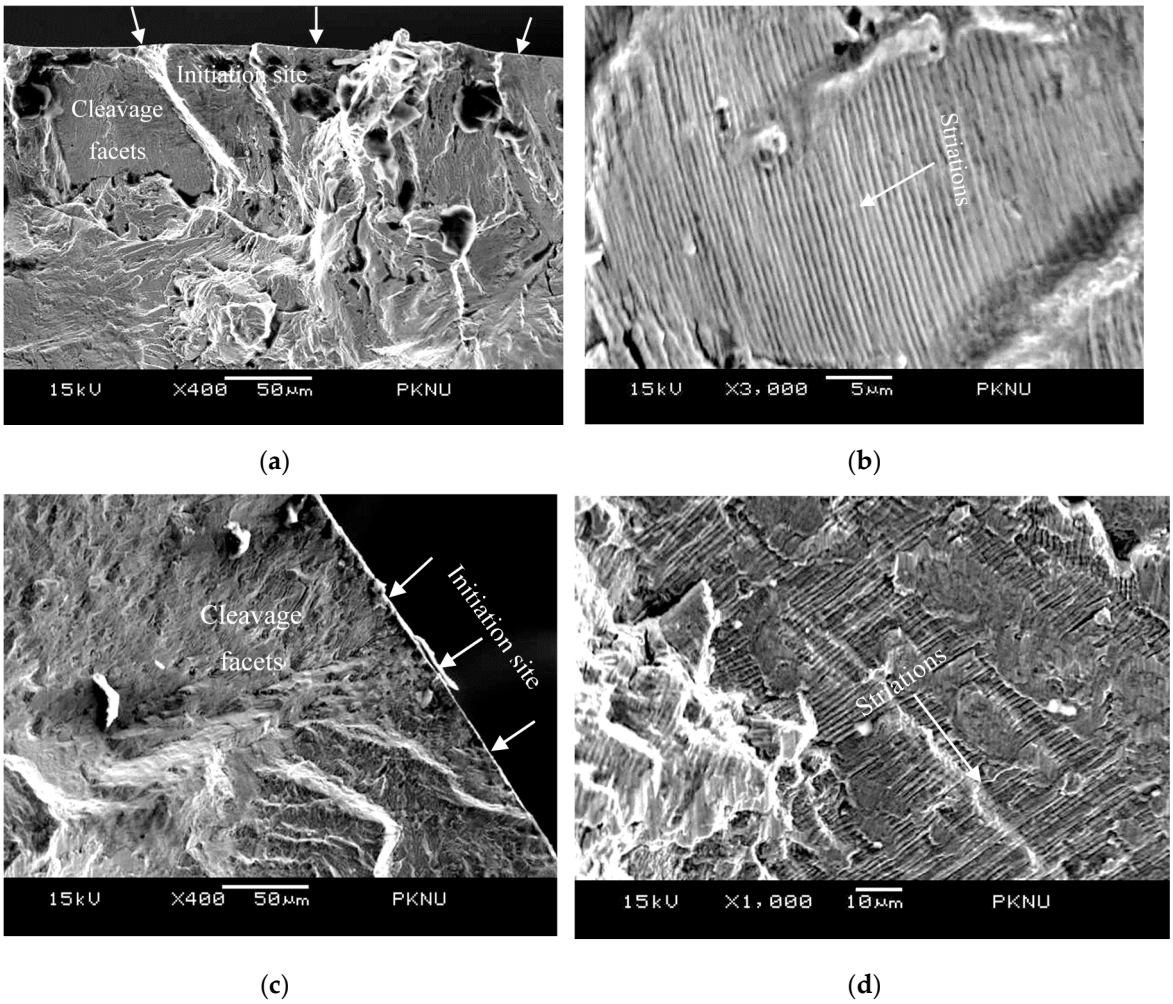

Figure 11. Typical SEM micrographs of the fractured surface for Alloy 617 weldments at 0.6% total strain range: (**a**,**b**) Room temperature; (**c**,**d**) 800 °C condition.

4. Conclusions

A fully reversed ($R_\varepsilon = -1$) total axial strain-controlled LCF tests of the Alloy 617 (INCONEL 617) weldments fabricated by GTAW process were conducted at room temperature and 800 °C in the air, with a total strain range of 0.6, 0.9, 1.2, and 1.5%. The following key conclusions are drawn:

1. The increasing of strain ranges and temperature condition resulted in a reduction of fatigue life. From the results, we can deduce that the higher plastic strain deformation and the material ductility of the 800 °C testing conditions have a major role in the shorter fatigue life.
2. For room temperature conditions, initial hardening was observed below 200 cycles, after that softening was observed until failure. Meanwhile, the 800 °C condition distinctly showed a cyclic hardening for the major portion of the fatigue life. In the 800 °C condition, we synchronously noticed the serrated flows on the tension-compression stresses at all testing conditions as dynamic strain aging (DSA) phenomena. Since the DSA-induced work hardening process due to atoms interactions may cause the rapid crack propagation, the fatigue life will also decrease in the regime of DSA.
3. The observed LCF life was well characterized by the Coffin-Manson relationship, and they are well compared with previous works. The parameter of *c* slope typically varied from −0.5~−1.0, and, in this study, the *c* slope was obtained by −0.654 and −0.889 at room temperature and 800 °C conditions, respectively.
4. The LCF cracking in weldments occurred inside of the gauge section in the WM region, and showed a wedge-type crack with some deviations oriented at 45° to the loading direction. A transgranular crack initiation with some cleavage facets (stage I) and propagation with some striations (stage II) along with the interdendritic paths were observed.

Acknowledgments: The authors would like to recognize KAERI, and acknowledge that this research was supported by Nuclear Research & Development Program through the National Research Foundation of Korea (NRF) funded by the Ministry of Science, ICT & Future Planning (NRF-2015M2A8A2021963).

Author Contributions: Seon Jin Kim formulated this research with cooperation from Woo Gon Kim and Eung Seon Kim (KAERI). Rando Tungga Dewa performed the experiment works, with the help of Seon Jin Kim, interpreted the results, prepared and revised the manuscript. All co-authors contributed to manuscript proof and submissions.

Conflicts of Interest: The authors declare no conflict of interest.

References

1. Kim, W.G.; Park, J.Y.; Ekaputra, I.M.W.; Kim, S.J.; Kim, M.H.; Kim, Y.W. Creep deformation and rupture behavior of Alloy 617. *Eng. Fail. Anal.* **2015**, *58*, 441–451. [CrossRef]
2. Kim, W.G.; Yin, S.N.; Kim, Y.W.; Ryu, W.S. Creep behaviour and long-term creep life extrapolation of alloy 617 for a very high temperature gas-cooled reactor. *Trans. Indian Inst. Met.* **2010**, *63*, 145–150. [CrossRef]
3. Wright, J.K.; Carroll, L.J.; Wright, R.N. *Creep and Creep-Fatigue of Alloy 617 Weldments*; Annual Report Idaho National Laboratory: Fremont, CA, USA; August; 2014.
4. Kim, S.J.; Dewa, R.T.; Kim, W.G.; Kim, M.H. Cyclic Stress Response and fracture behaviors of Alloy 617 base metal and weldments under LCF loading. *Adv. Mater. Sci. Eng.* **2015**, *2015*. [CrossRef]
5. Kim, S.J.; Choi, P.H.; Dewa, R.T.; Kim, W.G.; Kim, M.H. Low cycle fatigue properties of Alloy 617 base metal and weldment at room temperature. *Proc. Mater. Sci. Eur. Conf. Fract.* **2014**, *3*, 2201–2206.
6. Prasad Reddy, G.V.; Sandhya, R.; Valsan, M.; Bhanu Sankara Rao, K. High temperature low cycle fatigue properties of 316(N) weld metal and 316L(N)/316(N) weldments. *Int. J. Fatigue* **2008**, *30*, 538–546. [CrossRef]
7. Bhanu Sankara Rao, K.; Schiffers, H.; Schuster, H.; Nickel, H. Influence of time and temperature dependent processes on strain controlled LCF behavior of Alloy 617. *Metall. Trans. A* **1988**, *19A*, 359–371.
8. Meurer, H.P.; Gnirss, G.K.H.; Mergler, W.; Raule, G.; Schuster, H.; Ullrich, G. Investigations on the fatigue behavior of high temperature gas cooled reactor components. *Nucl. Technol.* **1984**, *66*, 315–323.
9. Totemeier, T.C.; Tian, H. Creep-fatigue interactions in INCONEL 617. *Mater. Sci. Eng. A* **2007**, *468–470*, 81–87. [CrossRef]

10. Carroll, L.J.; Cabet, C.; Wright, R.N. The role of environment on high temperature creep-fatigue behaviour of Alloy 617. In Proceedings of the ASME 2010 Pressure Vessel and Piping Division Conference, Bellevue, WA, USA, 18–22 July 2010; pp. 907–916.
11. Wright, J.K.; Carroll, L.J.; Simpson, J.A.; Wright, R.N. Low cycle fatigue of Alloy 617 at 850 °C and 950°C. *J. Eng. Mater. Technol. ASME* **2013**, *135*, 1–8. [CrossRef]
12. Chen, X.; Sokolov, M.A.; Sham, S.; Erdman, D.L.; Busby, J.T.; Mo, K.; Stubbins, J.F. Experimental and modeling results of creep-fatigue life of Inconel 617 and Haynes 230 at 850 °C. *J. Nucl. Mater.* **2013**, *432*, 94–101. [CrossRef]
13. Kewther Ali, M.; Hashmi, M.S.J.; Yilbas, B.S. Fatigue properties of the refurbished INCO-617 Alloy. *J. Mater. Process. Technol.* **2001**, *118*, 45–49. [CrossRef]
14. Totemeier, T.C. High-temperature creep-fatigue of Alloy 617 base metal and weldments. In Proceedings of ASME 2007 Pressure Vessels and Piping Conference, San Antonio, TX, USA, 22–26 July 2007; pp. 255–260.
15. ASTM E 606-92. Standard Practice for Strain-Controlled Fatigue Testing. In *Annual Book of ASTM Standards*; ASTM International: Baltimore, MD, USA, 2002; p. 569.
16. Hong, J.D.; Lee, J.; Jang, C.; Kim, T.S. Low cycle fatigue behavior of alloy 690 in simulated PWR water—Effects of dynamic strain aging and hydrogen. *Mater. Sci. Eng. A* **2014**, *611*, 37–44. [CrossRef]
17. Gallo, P.; Berto, F.; Lazzarin, P. High temperature fatigue tests of notched specimens made of titanium Grade 2. *Theor. Appl. Fract. Mech.* **2015**, *76*, 27–34. [CrossRef]
18. Louks, R.; Susmel, L. The linear-elastic Theory of Critical Distances to estimate high-cycle fatigue strength of notched metallic materials at elevated temperatures. *Fatigue Fract. Eng. Mater. Struct.* **2015**, *38*, 629–940. [CrossRef]
19. Hong, S.G.; Lee, S.B. Mechanism of dynamic strain aging and characterization of its effect on the low-cycle fatigue behavior in type 316L stainless steel. *J. Nucl. Mater.* **2005**, *340*, 307–314. [CrossRef]